American Mineralogist, Volume 75, pages 601–619, 1990

Activity diagrams for clinoptilolite: Susceptibility of this zeolite to further diagenetic reactions

Teresa S. Bowers, Roger G. Burns
Department of Earth, Atmospheric, and Planetary Sciences, Massachusetts Institute of Technology, Cambridge, Massachusetts 02139, U.S.A.

Abstract

Clinoptilolite is the predominant zeolite in diagenetically altered volcanic rocks at Yucca Mountain, Nevada, having formed by posteruptive reactions of ground water with vitric tuffs in the pyroclastic deposits. Compositional variations of clinoptilolites in the fractured and zeolitized tuffs not presently in contact with ground water and the vulnerability of zeolites to burial diagenesis raise questions about the long-term stability of clinoptilolite. Equilibrium activity diagrams were calculated for clinoptilolite solid solutions in the seven-component system Ca-Na-K-Mg-Fe-Al-Si plus H_2O, employing available thermodynamic data for related minerals, aqueous species, and water. Stability fields are portrayed graphically on plots of $\log(a_{Na^+}/a_{H^+})$ versus $\log(a_{Ca^{2+}}/(a_{H^+})^2)$, assuming the presence of potassium feldspar, saponite, and hematite, and using ranges of activities for SiO_2 and Al^{3+} defined by the saturation limits for several silica polymorphs, gibbsite, kaolinite, and pyrophyllite. Formation of clinoptilolite is favored by higher SiO_2 activities than allowed for by the presence of quartz, thus accounting for the coexistence of clinoptilolite with opal-CT in zeolitized vitric tuffs. The clinoptilolite stability field broadens with increasing atomic substitution of Ca for Na, and K for Ca, reaches a maximum for intermediate activities of dissolved Al, and decreases with increasing temperature. The thermodynamic calculations show that ground water of the sodium-bicarbonate type, such as reference J-13 well water collected from fractured devitrified tuffs at the adjacent Nevada Nuclear Test Site, is approximately in equilibrium at 25 °C with calcite and several zeolites, including heulandite and calcic clinoptilolite. Mg-rich clinoptilolites are stabilized in ground water depleted in Ca^{2+}. Decreasing Al^{3+} activities result in the association of clinoptilolite with calcite and opal-CT observed in weathered zeolitized vitric tuffs at Yucca Mountain. The activity diagrams indicate that prolonged diagenetic reactions with ground water depleted in Al, enriched in Na or Ca, and heated by the thermal envelope surrounding buried nuclear waste may eliminate sorptive calcic clinoptilolites in fractured tuffs and underlying basal vitrophyre.

Introduction

Clinoptilolite, ideally $(Na,K,Ca_{0.5})_6Si_{30}Al_6O_{72}\cdot 24H_2O$, is an abundant zeolite in diagenetically altered rhyolite tuffs, where it forms by posteruptive reactions of hydrated glass shards (Hay, 1966; Hay and Sheppard, 1977; Iijima, 1975, 1980). Silicic air-fall and ash-flow tuffs are the predominant rocks at Yucca Mountain, Nevada, the site of the proposed repository for burial of high-level nuclear waste (U.S. DOE, 1988). The repository horizon at this site is a densely welded and devitrified tuff unit underlain by a basal vitrophyre and vitric to zeolitized non-welded tuffs containing high proportions of clinoptilolite (Broxton et al., 1987). Because of its favorable cation exchange reactions, clinoptilolite is advocated as one mineral in the tuffaceous deposits capable of immobilizing several of the soluble cations and being an effective barrier to radionuclide migration (Ogard et al., 1984), should water entering the repository cause leakage of fission products.

Clinoptilolites analyzed in drill-core samples throughout Yucca Mountain and its vicinity display wide compositional variations, particularly in fractures adjacent to the repository horizon in the Topopah Spring Member of the Paintbrush Tuff unit and in underlying zeolitized vitric tuffs (Broxton et al., 1987). In the vadose zone beneath Yucca Mountain, clinoptilolites with high Ca and Mg contents line fractures in the Topopah Spring Member (Carlos, 1985; Broxton et al., 1986, 1987). In underlying bedded tuffs, the clinoptilolites display regional and depth variations (Broxton et al., 1986, 1987). On the western side of Yucca Mountain the clinoptilolites are Na-K-bearing and become Na-rich with depth. To the east, the clinoptilolites are Ca-K-bearing and become Ca-rich with depth. Such compositional variations are portrayed in

0003–004X/90/0506–0601$02.00

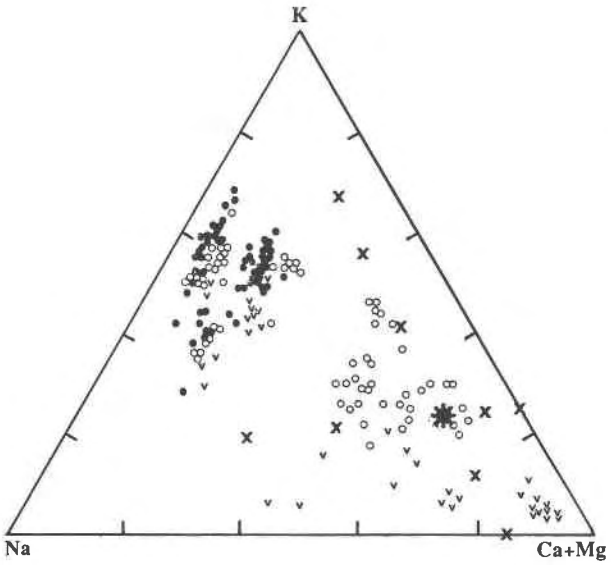

Fig. 1. Triangular diagram showing compositional variations of clinoptilolite and heulandites (modified from Broxton et al., 1986). Superimposed on data for these zeolites in the unsaturated zone at Yucca Mountain, Nevada, are compositions used in the thermodynamic calculations: ●, ○ western and eastern parts of the repository block (Broxton et al., 1986); V lining fractures in and below the proposed repository horizon (Carlos, 1985); * measured calorimetrically (Hemingway and Robie, 1984); X different atomic substitutions used to calculate activity diagrams in Fig. 11.

Figure 1. Similar regional and depth variations occur in zeolitized tuffs at the adjacent Nevada Test Site (Hoover, 1968). Such compositional variations of clinoptilolite not presently in contact with ground water and the susceptibility of zeolites to further diagenetic reactions (Moncure et al., 1981; Smyth, 1982) suggest that the long-term thermodynamic stability of clinoptilolite should be examined.

Although the Topopah Spring Member tuff and underlying zeolitized tuffs lie in the unsaturated or vadose zone, well above the present-day water table beneath Yucca Mountain, these formations dip to the east so that at the location of the nearest water-supply well, designated J-13 and located 6 km to the east at Jackass Flat on the Nevada Test Site, the Topopah Spring Member lies beneath the water table. The major producing horizon for J-13 well water is a highly fractured interval within the Topopah Spring Member (Delany, 1985). The chemical composition of the ground water obtained from well J-13 has been monitored for several years (Daniels et al., 1982; Bish et al., 1984; Kerrisk, 1987) and serves as a standard in laboratory experiments and geochemical modeling studies for the Yucca Mountain exploration block (e.g., Oversby, 1985; Delany, 1985; Knauss et al., 1985a, 1985b; Moore et al., 1986; Thomas, 1987; U.S. DOE, 1988, p. 4–51). Whether J-13 well water is of an appropriate composition for the prediction of authigenic mineral reactions in the unsaturated zone beneath Yucca Mountain requires critical evaluation.

In order to assess the stability limits of clinoptilolite and its vulnerability to changes of ground water chemistry relative to the composition of J-13 well water, equilibrium activity diagrams have been calculated for clinoptilolite solid solutions in the system Ca-Na-K-Mg-Fe-Al-Si-H_2O, employing available thermodynamic data for oxide and aluminosilicate phases. Although low-temperature processes are subject to many kinetically controlled variables, the assumption of thermodynamic equilibrium provides a reference from which to assess observed mineral relations. Results reported here indicate that authigenic minerals such as clinoptilolite modify and are modified by ground-water compositions.

Calculations of activity diagrams

Sources of thermodynamic data

The method for calculating activity diagrams is described in Bowers et al. (1984), who also tabulated thermodynamic data for many of the phases considered here. Thermodynamic data for zeolites including clinoptilolite, heulandite, natrolite, scolecite, and mesolite are provided by calorimetric measurements made by Johnson et al. (1982, 1983, 1985) and Hemingway and Robie (1984). Table 1 lists formulae of all of the minerals considered in this study. Note that several of these minerals (notably laumontite, stilbite, and chabazite) were found not to exhibit stability fields within the pressure, temperature, and compositional ranges of the calculations.

The clinoptilolite measured by Hemingway and Robie (1984) from altered tuffs of the Big Sandy Formation, Mohave County, Arizona (Sheppard and Gude, 1973) was formulated by them as

$$Na_{0.56}K_{0.98}Ca_{1.50}Mg_{1.23}Fe_{0.3}Al_{6.7}Si_{29}O_{72}\cdot 22H_2O,$$

with Si/Al = 4.33 and (Na + K) > Ca. The heulandite measured by Johnson et al. (1985) was formulated as

$$Ca_{0.585}Sr_{0.175}Ba_{0.063}Na_{0.383}K_{0.132}Si_{6.835}Al_{2.165}O_{18}\cdot 6.0H_2O,$$

with Si/Al = 3.16 and (Ca + Sr + Ba) > (Na + K). Note that clinoptilolite and heulandite are isostructural, and a continuous solid-solution series exists between the two minerals. By convention, the compositional boundary for clinoptilolite is determined by the ratios Si/Al $\geq$ 4 and (Na + K) $\geq$ Ca, whereas heulandite has Si/Al < 4 and Ca > (Na + K). As indicated in Figure 1, the composition of the clinoptilolite for which thermodynamic data are available resembles those of the (Ca + Mg)-rich zeolites that line fractures in the Topopah Spring Member and are present in underlying zeolitized vitric tuffs, particularly beneath the northeastern block of Yucca Mountain (Broxton et al., 1987).

Several minerals of interest in this study, including clinoptilolite, have measured heat-capacity and entropy data, but no Gibbs free energy of formation at 25 °C (ΔG_f°). When this is the case, free energies can be estimated by

Table 1. Minerals and formulas

Quartz	SiO_2
Amorphous silica	SiO_2
Gibbsite	$Al(OH)_3$
Diaspore	$AlO(OH)$
Kaolinite	$Al_2Si_2O_5(OH)_4$
Pyrophyllite	$Al_2Si_4O_{10}(OH)_2$
Wollastonite	$CaSiO_3$
Grossular	$Ca_3Al_2Si_3O_{12}$
Anorthite	$CaAl_2Si_2O_8$
Gehlinite	$Ca_2Al_2SiO_7$
Prehnite	$Ca_2Al_2Si_3O_{10}(OH)_2$
Margarite	$CaAl_4Si_2O_{10}(OH)_2$
Ca end-member beidellite	$Ca_{0.165}Al_2(Al_{0.33}Si_{3.67}O_{10})(OH)_2$
Lawsonite	$CaAl_2Si_2O_7(OH)_2 \cdot H_2O$
Wairakite	$CaAl_2Si_4O_{12} \cdot 2H_2O$
Laumontite	$CaAl_2Si_4O_{12} \cdot 4H_2O$
Chabazite	$CaAl_2Si_4O_{12} \cdot 6H_2O$
Ca end-member phillipsite	$CaAl_2Si_5O_{14} \cdot 5H_2O$
Scolecite	$CaAl_2Si_3O_{10} \cdot 3H_2O$
Epistilbite	$CaAl_2Si_6O_{16} \cdot 5H_2O$
Heulandite	$CaAl_2Si_7O_{18} \cdot 6H_2O$
Albite	$NaAlSi_3O_8$
Nepheline	$NaAlSiO_4$
Paragonite	$NaAl_2(AlSi_3O_{10})(OH)_2$
Na end-member beidellite	$Na_{0.33}Al_2(Al_{0.33}Si_{3.67}O_{10})(OH)_2$
Na end-member phillipsite	$Na_2Al_2Si_5O_{14} \cdot 5H_2O$
Analcime	$NaAlSi_2O_6 \cdot H_2O$
Natrolite	$Na_2Al_2Si_3O_{10} \cdot 2H_2O$
Mordenite	$NaAlSi_5O_{12} \cdot 3H_2O$
Potassium feldspar	$KAlSi_3O_8$
Kalsilite	$KAlSiO_4$
Muscovite	$KAl_2(AlSi_3O_{10})(OH)_2$
K end-member beidellite	$K_{0.33}Al_2(Al_{0.33}Si_{3.67}O_{10})(OH)_2$
K end-member phillipsite	$K_2Al_2Si_5O_{14} \cdot 5H_2O$
Phillipsite	$Na_{1.08}K_{0.80}Al_{1.88}Si_{6.12}O_{16} \cdot 6H_2O$
H end-member beidellite	$H_{0.33}Al_2(Al_{0.33}Si_{3.67}O_{10})(OH)_2$
Stilbite	$NaCa_2Al_5Si_{13}O_{36} \cdot 14H_2O$
Mesolite	$Na_{0.676}Ca_{0.657}Al_{1.99}Si_{3.01}O_{10} \cdot 2.647H_2O$
Clinoptilolite	$(Na_{0.58}K_{0.98}Ca_{1.5}Mg_{1.23})(Al_{6.7}Fe_{0.3})Si_{29}O_{72} \cdot 22H_2O$
Ca end-member saponite	$Ca_{0.165}Mg_3(Al_{0.33}Si_{3.67}O_{10})(OH)_2$
Hematite	Fe_2O_3

various component-summation methods. The method of Chen (1975) was used here for Na end-member phillipsite, K end-member phillipsite, and (Na,K) end-member phillipsite. This method involves summing several sets of components, including oxides, simple silicates, and components of similar structural type. The resulting free-energy determinations are fit with an exponential curve that asymptotically approaches a low value that is used as ΔG_f°. Chen (1975) reported an estimated error in ΔG_f° obtained in this manner of less than 0.6% for a number of minerals when compared to their experimental values. An attempt was made to estimate free energies for the clinoptilolite formulated by Hemingway and Robie (1984) and for end-member heulandite, Ca end-member phillipsite, stilbite, chabazite, and epistilbite formulated in Table 1 using Chen's (1975) method. Clinoptilolite and end-member heulandite were treated as separate phases on the basis of different Si-Al ratios even though a continuous solid-solution series exists between the two minerals. The independent estimates of ΔG_f° from summing various components for clinoptilolite and each of the end-member minerals listed above did not fall along exponential curves, but decreased linearly such that an exponential fit could not be made. Chen (1975) noted a similar difficulty with some minerals. The free energy of formation for these minerals was therefore taken as the lowest value obtained from the various component-summation schemes and generally involved summing over zeolite and other hydrous components, including natrolite, scolecite, K end-member phillipsite, brucite, kaolinite, quartz, and hematite. The error associated with this method will be somewhat higher than the 0.6% estimated by Chen (1975). All estimated ΔG_f° and ΔH_f° data used in this study are in Table 2. In addition, since alkali-rich mordenite fre-

Table 2. Estimated free energies and enthalpies of some zeolites*

	$\Delta G_f^\circ(298)$ (cal/mol)	$\Delta H_f^\circ(298)$ (cal/mol)
Na end-member phillipsite	−1 851 376	−2 003 469
K end-member phillipsite	−1 871 460	−2 025 549
Ca end-member phillipsite	−1 860 596	−2 010 073
Phillipsite	−2 112 851	−2 294 159
Mordenite	−1 465 647	—
Epistilbite	−2 065 242	−2 234 763
Chabazite	−1 712 637	−1 866 861
Stilbite	−4 833 571	−5 247 477
Heulandite	−2 326 575	−2 519 882
Clinoptilolite	−9 057 789	−9 811 932

* Mineral formulas given in Table 1.

TABLE 3. Estimated free energies for compositionally variable clinoptilolite

	$\Delta G_f^\circ(298)$ (cal/mol)
$(Na_{0.56}K_{0.98}Ca_{1.5}Mg_{1.23})$-$(Al_{6.7}Fe_{0.3})Si_{29}O_{72}\cdot 22H_2O$	−9 057 789
Na-Ca substitution	
$Na_{1.56}Ca_{1.0}$	−9 052 517
$Na_{2.56}Ca_{0.5}$	−9 047 244
$Na_{3.56}$	−9 041 972
$Na_{0.28}Ca_{1.64}$	−9 059 265
$Ca_{1.78}$	−9 060 742
K-Ca substitution	
$K_{1.98}Ca_{1.0}$	−9 068 653
$K_{2.98}Ca_{0.5}$	−9 079 517
$K_{3.98}$	−9 090 381
$K_{0.5}Ca_{1.74}$	−9 052 574
$Ca_{1.99}$	−9 047 142
Ca-Mg substitution	
$Ca_{0.73}Mg_{2.0}$	−9 036 211
$Ca_{1.7}Mg_{1.03}$	−9 063 394
$Ca_{2.0}Mg_{0.73}$	−9 071 801
$Ca_{2.5}Mg_{0.23}$	−9 085 813
$Ca_{2.73}$	−9 092 259

quently coexists with clinoptilolite in zeolitized tuffs at Yucca Mountain (Sheppard et al., 1988), its ΔG_f° was also estimated by Chen's (1975) method. However, because no measured thermodynamic data are available for mordenite, this zeolite was used only in activity diagrams calculated at 25 °C, although, as noted later, mordenite occurs at elevated temperatures in hydrothermal environments (Sturchio et al., 1989). The end-member heulandite formulated in Table 1 was the only one used in the calculations presented here because, as noted earlier, the specimen measured by Johnson et al. (1985) contained Ba and Sr components not included in this study.

Previous estimates of thermodynamic properties of clinoptilolite, heulandite, and mordenite were made by Kerrisk (1983). However, those calculations were made prior to recently published calorimetric data (Johnson et al., 1982, 1983, 1985; Hemingway and Robie, 1984). Direct comparisons between Kerrisk's (1983) estimates and those presented here cannot be made because he estimated equilibrium constants of specific hydrolysis reactions rather than free energies of formation of the minerals themselves.

Table 3 contains estimated free energies of formation for compositionally variable clinoptilolites. Independent substitutions of Na for Ca, K for Ca, and Ca for Mg were allowed, where constant charge balance and Si/Al ratio of 4.33 are maintained. Corresponding ΔG_f° values for each of these derived compositions were estimated from the value given for clinoptilolite in Table 2 by a component-summation method using natrolite, scolecite, and H_2O for Na-Ca substitution; K end-member phillipsite, scolecite, quartz, and H_2O for K-Ca substitution; and scolecite, brucite, kaolinite, and quartz for Ca-Mg substitution. These correction mechanisms resulted in lower ΔG_f° values for Ca over Na, K over Ca, and Ca over Mg-rich clinoptilolites.

Composition of ground water

Because the Topopah Spring Member tuff is the major producing horizon for water pumped from the J-13 well, it has been generally assumed (Oversby, 1985) that the composition of J-13 well water approximates the prevailing water chemistry of the proposed repository horizon in the same formation at Yucca Mountain even though the Topopah Spring Member there is in the unsaturated zone. As a result, J-13 well water continues to be widely used as the reference aqueous phase for calibrating numerous environmental parameters relevant to the Yucca Mountain repository horizon (Oversby, 1985; Delany, 1985; Knauss et al., 1985a, 1985b; Moore et al., 1986; Thomas, 1987; U.S. DOE, 1988, p. 4–51). The chemical composition of J-13 well water has been monitored for several years (Daniels et al., 1982; Kerrisk, 1987), and typical concentrations of dissolved species in it are summarized in Table 4. Small fluctuations in concentrations over time have been recorded, but the variations are minor compared with other variables in experiments in which J-13 well water was used (Daniels et al., 1982). However, during experiments in which J-13 well water was contacted with tuff samples of the Topopah Spring Member taken from a drill core at the appropriate region of main water production of the J-13 well, concentrations of many constituents changed slightly (Table 4), particularly Mg and Al, which decreased after three weeks at room temperature (Daniels et al., 1982). Moreover, filtration affected the compositions of some elements, particularly Fe, Al, and Mg, which were drastically reduced in samples passed through 0.05 μm Nuclepore membranes compared to those obtained from 0.45 μm Millipore filters (Daniels et al., 1982). The Al concentration, for example, decreased from ~40 mg/L (0.45 μm filter) to <0.01 mg/L (0.05 μm filter) (Daniels et al., 1982). The Al concentration of J-13 well water (0.012 mg/L) represents one of the lowest values reported for drill holes throughout Yucca Mountain (Ogard and Kerrisk, 1984).

Cation concentrations in solutions contacted with vitrophyre samples from the Topopah Spring Member at 152 °C showed significant increases of dissolved Si, Fe, Al, K, and Na and a decrease of dissolved Mg, which were attributed to dissolution of glass and precipitation of clays (Daniels et al., 1982). A specimen of zeolitized tuff reacted with J-13 well water at 152 °C showed marked dissolution of clinoptilolite and disappearance of mordenite and cristobalite (Daniels et al., 1982). In later experiments, Knauss et al. (1985a, 1985b) studied compositional changes of J-13 well water after reacting it with crushed tuff and polished wafer samples of the densely welded, devitrified ash-flow tuff in a drill core taken from the respository level in the Topopah Spring Member. The modal minerals of this horizon consist of ~98% microcrystalline sanidine-cristobalite-quartz and accessory (<2%) biotite-montmorillonite (Bish et al., 1984; Broxton et al., 1989). Reactions were performed over 2–3 months at temperatures of 90, 150, and 250 °C and pres-

TABLE 4. Chemical composition of J-13 well water (mg/L)

	A	B	C	D	E	F	G
Li	0.042	—	—	—	0.06	0.05	0.05
Na	43.9	55	58.5	44	45	51	54.1
K	5.11	7.5	5.58	4.4	5.3	4.9	6.4
Ca	12.5	11.5	6.46	13	11.5	14	11
Mg	1.92	1.1	0.315	2.0	1.76	2.1	0.95
Sr	0.035	—	—	—	—	0.05	0.002
Al	0.012	0.999	1.64	—	0.03	0.03	0.01
Fe	0.006	—	—	—	0.04	0.04	0.004
SiO_2	57.9	53	148	59	64.3	66	71.6
NO_3	9.6	9.0	9.5	8.7	10.1	5.6	—
F	2.2	2.3	2.4	2.2	2.1	2.2	—
Cl	6.9	7.2	7.4	—	6.4	7.5	—
HCO_3	125.3	178.8	61.0	120	143	120	—
SO_4	18.7	18.3	18.5	19	18.1	22	—
pH	7.6	7.27	6.97	7.5	6.9	7.1	—

A. Delany (1985).
B. J-13 reacted with TS tuff at 90 °C; Knauss et al. (1985a).
C. J-13 reacted with TS tuff at 150 °C; Knauss et al. (1985a).
D. Moore et al. (1986).
E. Ogard and Kerrisk (1984).
F. Daniels et al. (1982).
G. Daniels et al. (1982), after J-13 water reacted with TS tuff at 25 °C.

sures of 90–100 bars. Results from the experiments at 150 °C are in Table 4, where it can be seen that dissolved SiO_2 concentrations increase and are close to the cristobalite saturation value (Knauss et al., 1985a). Na also increased during the experiments, Ca and Mg decreased, and Al and K both increased rapidly and then decreased. These effects were attributed to dissolution of montmorillonite and precipitation of calcite and illite. The experiments at 90 and 250 °C produced similar results. Phases identified by scanning electron microscopy included illite, Mg-Ca or Fe-rich clays, gibbsite, calcite, and a pure SiO_2 phase considered to be cristobalite (Knauss et al., 1985a, 1985b).

Studies to determine compositional changes of ground water as it passes through the unsaturated zone in tuffaceous deposits have been conducted at Rainier Mesa, located 50 km to the north-northeast of Yucca Mountain (Benson, 1976; White et al., 1980). At Rainier Mesa welded and vitric tuffs overlie zeolitized tuffs, resembling the sequence of ash-flow tuffs at Yucca Mountain. Concentrations of Ca and Mg in interstitial waters decreased as a function of depth and were generally lower than those in J-13 well water, whereas opposite effects were observed for Na (Benson, 1976; White et al., 1980). The concentration of dissolved K was lower at depth, and that of SiO_2 higher, than J-13 well-water compositions, whereas Cl^- decreased and HCO_3^- increased with depth. The maximum compositional variations of the interstitial water occurred in alteration zones containing clinoptilolite and montmorillonite (Benson, 1976; White et al., 1980). Water seeping through fractures in tunnels beneath the zeolitized tuffs was HCO_3^--rich and had lower Ca, Mg, and SiO_2 contents, variable K concentrations, and higher Na concentrations than J-13 well water (Benson, 1976; White et al., 1980). The clinoptilolites along the fractures were Ca-Mg-K-rich, correlating with the depletion of these cations in the ground water, whereas the fracture-flow water was enriched in HCO_3^- relative to the more Cl^--rich interstitial water. Comparisons made with dissolution experiments on vitric and crystalline tuffs demonstrated the rapid release of Na and SiO_2 but the retention of K in glass-bearing tuffs, whereas dissolution of crystalline tuffs containing sanidine, quartz, biotite, and clinopyroxene phenocrysts and sanidine-cristobalite groundmass resulted in solutions rich in Ca, Mg, and HCO_3^- (White et al., 1980). White et al. (1980) thus concluded that fracture-water compositions, such as J-13 well water, are dominated by dissolution of vitric tuffs but are modified by infiltration through zeolitized tuffs.

The composition of J-13 well water not only plots in the field of the Rainier Mesa interstitial and fracture-flow waters, but analyses also lie in the middle of compositional ranges for ground water pumped from several wells throughout Yucca Mountain originating from various depths in the saturated zone (Ogard and Kerrisk, 1984) at temperatures rarely exceeding 40 °C. In the Yellowstone hydrothermal environment, downhole water compositions at 140 °C show appreciably higher concentrations of SiO_2, HCO_3^-, Na, and K, and lower Ca contents than the lower temperature J-13 well water (31 °C). Clinoptilolites there are enriched in K and Na but are depleted in Ca (Keith et al., 1978; Sturchio et al., 1989). These results, and the experimental observations described earlier, clearly show that zeolitized rhyolitic tuffs affect ground-water chemistry, and they suggest that compositional variability of clinoptilolites influence and are influenced by ground-water compositions. They also indicate that potassic clinoptilolites are stable to at least 140 °C.

Recently attempts were made to measure compositions of pore water extracted by triaxial compression of nonwelded tuffs from the unsaturated zone at Yucca Moun-

tain (Yang et al., 1988). The samples of extracted water have much higher Ca, Mg, K, Sr, Cl^-, SO_4^{2-}, and SiO_2 concentrations than J-13 well water, and the compositions of extracted water are influenced by changes of axial stress on the compressed tuffs. Unfortunately, pH, HCO_3^-, and dissolved Al data were not reported for these tuff samples. Consequently, the pore-water compositions could not be used in our thermodynamic calculations.

Representation of activity diagrams

A number of activity diagrams are presented here, initially for simple three-component systems and subsequently for the more complex multicomponent systems that are required for depicting stability fields of clinoptilolite in felsic rocks. The primary focus is on the clinoptilolite composition highlighted earlier for which thermodynamic data are available (Hemingway and Robie, 1984). Although the chosen three-component systems serve as a necessary reference for establishing stability fields for clinoptilolite in the multicomponent systems discussed later, they also may contain useful information for diagenetic reactions involving other zeolites in felsic and mafic rocks.

Systems of three and four components plus H_2O can be readily represented in two dimensions. For example, in the system Ca-Al-Si-H_2O, two components are selected for the x and y axes, all reactions are balanced with respect to a third component, and the activity of H_2O is fixed, commonly equal to one. A reaction between amorphous silica and heulandite can be represented by writing a hydrolysis reaction for each mineral:

$$SiO_{2(am)} = SiO_{2(aq)} \quad (1)$$

$$CaAl_2Si_7O_{18}\cdot 6H_2O + 8H^+ = Ca^{2+} + 2Al^{3+} + 7SiO_{2(aq)} + 10H_2O \quad (2)$$

Combining Reactions 1 and 2 and eliminating $SiO_{2(aq)}$ from the equations gives

$$CaAl_2Si_7O_{18}\cdot 6H_2O + 8H^+ = 7SiO_{2(am)} + Ca^{2+} + 2Al^{3+} + 10H_2O \quad (3)$$

An equilibrium constant as a function of pressure and temperature can be calculated from thermodynamic data for this reaction and is expressed as

$$\log K = 2\log(a_{Al^{3+}}/(a_{H^+})^3) + \log(a_{Ca^{2+}}/(a_{H^+})^2) \quad (4)$$

If the x and y axes are chosen as $\log(a_{Al^{3+}}/(a_{H^+})^3)$ and $\log(a_{Ca^{2+}}/(a_{H^+})^2)$, respectively, Reaction 4 is the equation of a line with a slope of -2 and a y intercept of log K that forms the boundary on an activity diagram between amorphous silica and heulandite (see Fig. 3a, discussed later). Similar calculations are performed for all mineral pairs, and the resulting intersecting lines form the boundaries of the phases that appear on the stability diagrams presented here.

Systems with more than four components plus H_2O are calculated in a similar manner, but with the inclusion of any additional minerals assumed to be at saturation to constrain additional components. For example, the system Ca-Na-Al-Si-H_2O might have Ca and Na on the axes, be balanced on Al, and have coexisting amorphous silica, as in Reaction 3. Alternatively, this four-component system could be balanced with respect to SiO_2 and have the Al component constrained by a saturation phase such as gibbsite:

$$CaAl_2Si_7O_{18}\cdot 6H_2O + 2H^+ = 2Al(OH)_3 + 7SiO_{2(aq)} + Ca^{2+} + 4H_2O \quad (5)$$

Gibbsite, however, provides a theoretical maximum activity of the Al^{3+} component that may not be desirable in all circumstances. Saturation with respect to any Al-bearing mineral in the four-component system can be assumed, although, if the chosen saturation phase includes the components plotted on the axes of the diagram, it will change the topology of the other fields. At Yucca Mountain, drill-core samples in the vadose zone contain opal and smectite as coexisting authigenic SiO_2 and Al^{3+}-bearing phases, respectively, with some authigenic potassium feldspar and minor amounts of cristobalite, quartz, and calcite (Broxton et al., 1987; Bish, 1989). These phases, together with the composition of J-13 well water (Table 4), serve to define the ranges of silica and Al^{3+} activities shown in Figure 2, which were used to construct the activity diagrams presented here. Thus, lines labeled D and H on Figure 2 represent the extremes of dissolved silica saturation limits corresponding to quartz and amorphous silica, respectively; cristobalite has an intermediate saturation level approximated by line E; line F corresponds to coexisting kaolinite and pyrophyllite; and line G is the activity of dissolved SiO_2 in J-13 well water. Similarly, for dissolved Al^{3+}, lines A, B, and C correspond to saturation values for coexisting amorphous silica plus pyrophyllite, coexisting pyrophyllite plus kaolinite, and gibbsite, respectively, and line I represents an arbitrarily low value of dissolved Al, which, as shown later, is consistent with the coexistence of opal, calcite, and clinoptilolite. Note that, although gibbsite, kaolinite, and pyrophyllite have not been reported at Yucca Mountain, their ideal end-member compositions serve as useful constraints for dissolved Al^{3+} and SiO_2 activities. Smectite, however, which is pervasive at Yucca Mountain (Bish, 1989), has a sheet silicate structure resembling pyrophyllite. If smectite were used to constrain Al activities, its value would fall into the general range for pyrophyllite, depending on the smectite composition. The reported analysis of Al in J-13 well water, 0.012 mg/L, which, as noted earlier, is one of the lowest concentrations reported for ground water at Yucca Mountain (Ogard and Kerrisk, 1984), is too high to be equilibrium-controlled. The fluid speciation program used to calculate cation activities (EQ3NR of Wolery, 1983) indicates that at the measured pH of J-13 well water (~7.5), dissolved Al occurs predominantly as $Al(OH)_4^-$, with a calculated equilibrium value for $[Al^{3+}]$ of $\sim 2 \times 10^{-11}$ M. Using an activity coefficient of ~0.6 for Al^{3+} gives a value for $\log(a_{Al^{3+}}/(a_{H^+})^3)$ of 9.6, significantly in excess of the gibbsite saturation value of approximate-

ly 7.9 (Fig. 2). This value is inconsistent with the equilibrium coexistence of J-13 well water and any of the observed mineral assemblages at Yucca Mountain and other areas for which dissolved Al concentration data are available, and it cannot be used to constrain calculations presented here. As noted earlier, a possible interpretation of this discrepancy is that the Al in J-13 well water contains unfiltered particulate matter that passes through membrane filters (Daniels et al., 1982). In calculating the activity diagrams, the activity of H_2O is taken to be unity, and the calcite boundary is added to appropriate diagrams by assuming a dissolved HCO_3^- content equivalent to that of J-13 well water (Table 4) and using the 90 °C and 150 °C analytical data in the activity diagrams calculated at 100 °C and 150 °C, respectively.

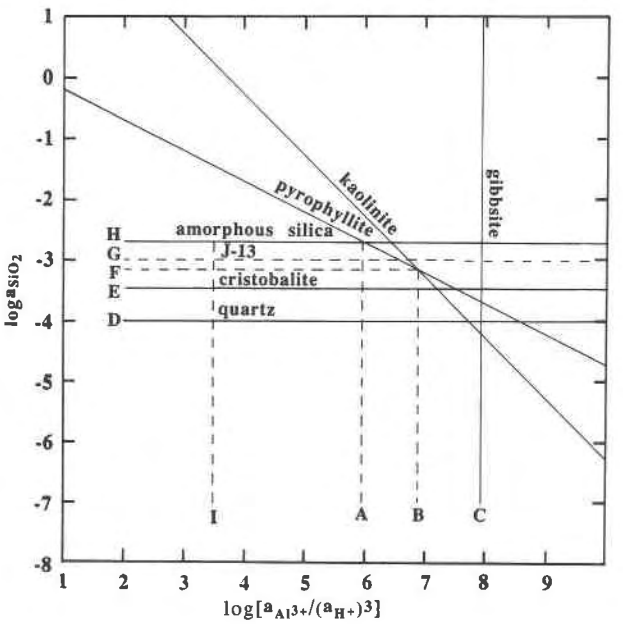

Fig. 2. Ranges of dissolved silica and aluminum activities used in the calculations of activity diagrams. Silica activities correspond to amorphous silica (H), J-13 well water (G), coexisting pyrophyllite-kaolinite-saturated solution (F), cristobalite-saturated solution (E), and quartz-saturated solution (D). Al activities are those for solutions saturated by assemblages of pyrophyllite + amorphous silica (A), pyrophyllite-kaolinite (B), and gibbsite (C) and an arbitrary low value (I).

Results

Diagrams of systems of three components plus H_2O

A series of diagrams of systems of three components plus H_2O are shown in Figures 3 to 5 for the systems Ca-Al-Si, Na-Al-Si, and K-Al-Si, respectively. All of these diagrams are balanced with respect to SiO_2. Quartz has been suppressed throughout the calculations described here in favor of amorphous silica because opal is the commonly observed authigenic SiO_2 phase in zeolitized ash-flow tuffs at Yucca Mountain (Broxton et al., 1986, 1987; Bish, 1989). As a result, each of the diagrams in Figures 3–5 has amorphous silica as the stable phase in the bottom left corner. Amorphous silica occupies a relatively smaller stability field than would quartz, had quartz not been suppressed. Figures 3a–3c illustrate the changes in phase relations for the system Ca-Al-Si with increasing temperatures at 25, 100, and 200 °C with pressures corresponding to the steam-saturation curve. Note that the heulandite field at 25 °C is replaced by Ca end-member phillipsite at higher temperatures. The scolecite field decreases in size with increasing temperature, and this zeolite is no longer stable at 200 °C (Fig. 3c). The field of Ca end-member beidellite apparent at 200 °C may exist at lower temperatures as well but does not appear in Figures 3a and 3b, possibly because of inaccuracies in the thermodynamic data for Ca end-member beidellite or adjacent phases. The stable limits of these and other activity diagrams described later are delineated by the dashed lines labeled gibbsite (or diaspore at 200 °C) and calcite. Higher Al or Ca activities can only result from supersaturation of the fluid with respect to these phases. As noted earlier, J-13 well water is unconstrained on the Al axis because its measured Al content cannot be reconciled with existing thermodynamic data. It is apparent from Figures 3a and 3b that in the simple Ca-Al-Si system J-13 well water is somewhat undersaturated with respect to calcite at 25 °C and would be slightly oversaturated at 100 °C.

Activity diagrams for the system Na-Al-Si are illustrated in Figures 4a and 4b. The 25 °C diagram (Fig. 4a) contains a stability field for mordenite. However, owing to lack of thermodynamic data for mordenite, this zeolite was not included in high-temperature calculations in Figure 4b. Its absence from Figure 4b is not indicative of stability limits for mordenite; indeed, mordenite occurs at ~170 °C in drill holes throughout the Yellowstone geothermal system (Keith et al., 1978; Sturchio et al., 1989). Thus, in the absence of mordenite the stability field of albite widens at 100 °C and Na end-member beidellite also becomes stable (Fig. 4b). Figures 5a and 5b show activity diagrams for the system K-Al-Si at 25 °C and 100 °C in which K end-member phillipsite is joined by potassium feldspar at high temperatures. J-13 well water is consistent with equilibrium with respect to either mordenite or albite (Fig. 4) and either K end-member phillipsite or potassium feldspar (Fig. 5).

Multicomponent diagrams

Figures 3 to 5 provide simplified activity diagrams used as references for comparison with the more complex systems of four and five components plus H_2O necessary for plotting the stability fields of clinoptilolite. Figures 6–9 are activity diagrams for the system Ca-Na-K-Al-Si. Values of $\log(a_{Na^+}/a_{H^+})$ and $\log(a_{Ca^{2+}}/(a_{H^+})^2)$ are plotted on the x- and y-axes, respectively, in each diagram. Either Al (Figs. 6 and 7) or Si (Figs. 8 and 9) has been used as the balancing component. In each case, two additional components need to be specified. The component K^+ is constrained by assuming the presence of potassium feldspar,

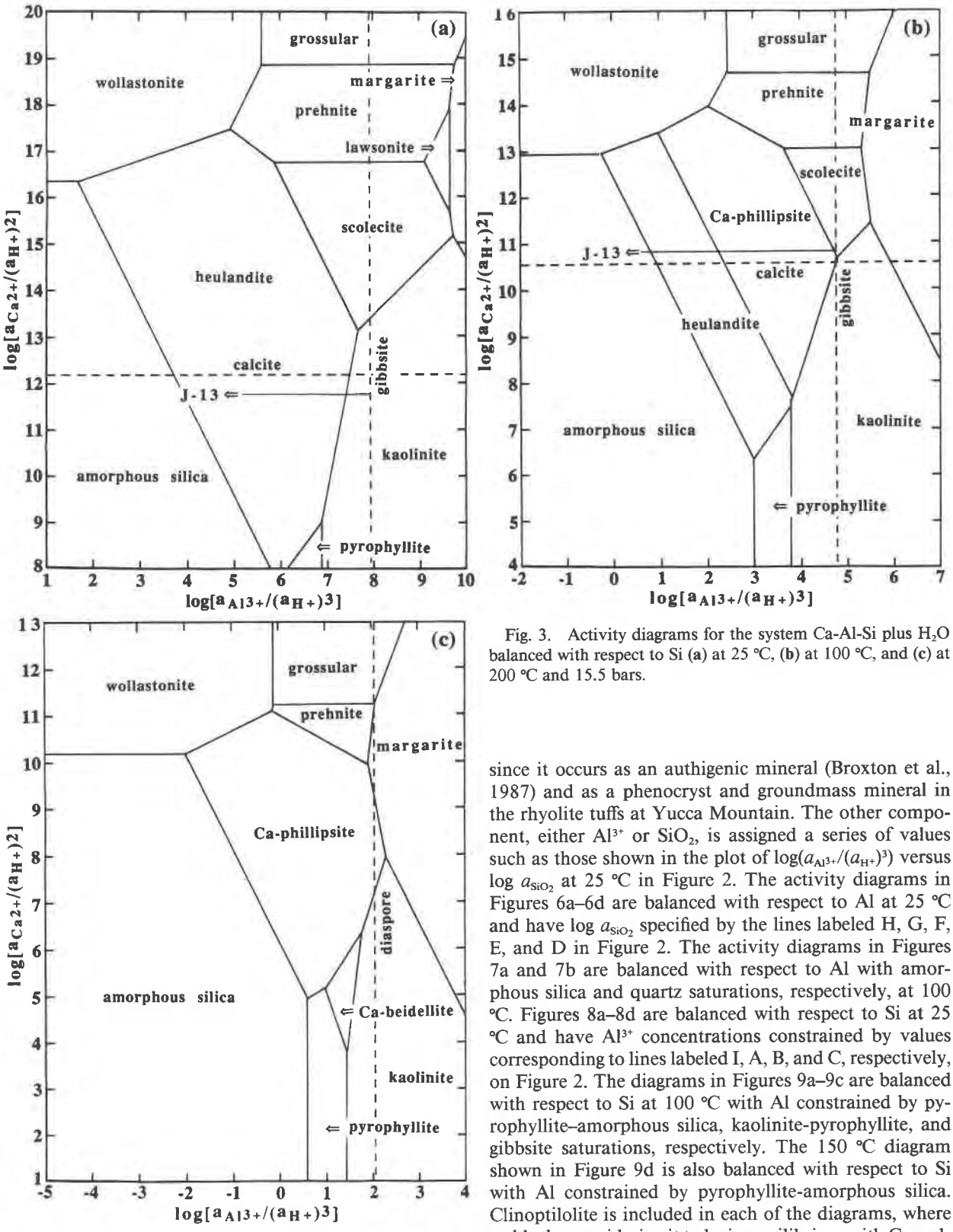

Fig. 3. Activity diagrams for the system Ca-Al-Si plus H_2O balanced with respect to Si (**a**) at 25 °C, (**b**) at 100 °C, and (**c**) at 200 °C and 15.5 bars.

since it occurs as an authigenic mineral (Broxton et al., 1987) and as a phenocryst and groundmass mineral in the rhyolite tuffs at Yucca Mountain. The other component, either Al^{3+} or SiO_2, is assigned a series of values such as those shown in the plot of $\log(a_{Al^{3+}}/(a_{H^+})^3)$ versus $\log a_{SiO_2}$ at 25 °C in Figure 2. The activity diagrams in Figures 6a–6d are balanced with respect to Al at 25 °C and have $\log a_{SiO_2}$ specified by the lines labeled H, G, F, E, and D in Figure 2. The activity diagrams in Figures 7a and 7b are balanced with respect to Al with amorphous silica and quartz saturations, respectively, at 100 °C. Figures 8a–8d are balanced with respect to Si at 25 °C and have Al^{3+} concentrations constrained by values corresponding to lines labeled I, A, B, and C, respectively, on Figure 2. The diagrams in Figures 9a–9c are balanced with respect to Si at 100 °C with Al constrained by pyrophyllite–amorphous silica, kaolinite-pyrophyllite, and gibbsite saturations, respectively. The 150 °C diagram shown in Figure 9d is also balanced with respect to Si with Al constrained by pyrophyllite-amorphous silica. Clinoptilolite is included in each of the diagrams, where stable, by considering it to be in equilibrium with Ca end-member saponite (smectite) and hematite to account for

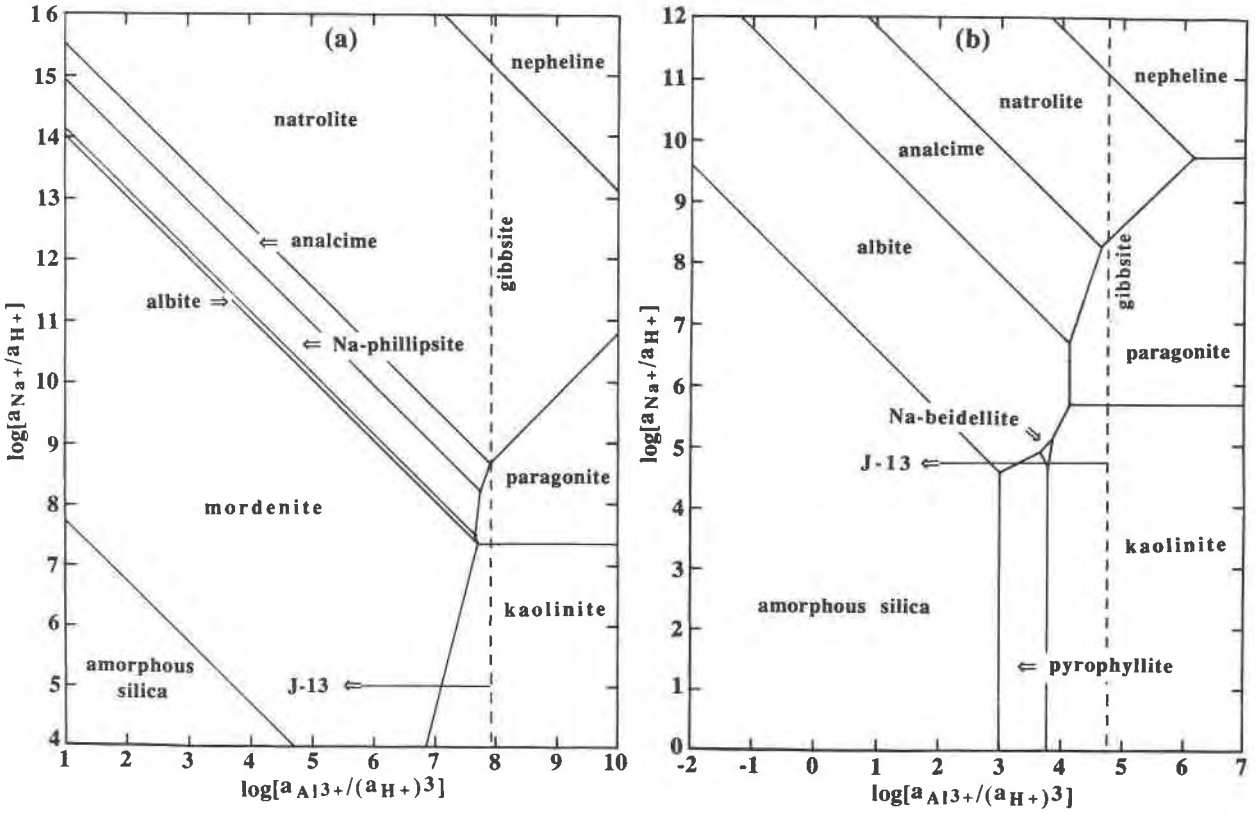

Fig. 4. Activity diagrams for the system Na-Al-Si plus H_2O balanced with respect to Si (**a**) at 25 °C; and (**b**) at 100 °C.

the small amounts of Mg and Fe found in the clinoptilolite specimen measured by Hemingway and Robie (1984). As noted earlier, limited thermodynamic data for mordenite enable its stability field to be shown on diagrams at 25 °C only. On all of the activity diagrams shown in Figures 6–9, calcite is plotted with a dashed line by assuming a bicarbonate ion content comparable to J-13 well water, and the circular symbol labeled J-13 corresponds to Ca and Na activities of this reference ground water.

By comparing the activity diagrams shown in Figures 6–9 through changing temperature, or for different activities of Al or Si, trends in the relative stabilities of various zeolite phases may be recognized easily. For example, Figure 6 shows that (1) clinoptilolite is stable at high activities of silica and its field decreases with decreasing silica activity, (2) the heulandite field also diminishes with silica activity but still remains when cristobalite is present, correlating with heulandite + cristobalite assemblages found in some drill cores at Yucca Mountain, (3) the mesolite stability field, which exists at low activities of silica, narrows and then disappears with increasing silica activity, and (4) at low silica activities, scolecite and albite are stabilized relative to heulandite and mordenite, respectively.

The effects of temperature can be seen by comparing Figure 6a (solid lines) with Figure 7a (corresponding to amorphous silica saturation) and Figure 6d with Figure 7b (quartz saturation), where it is apparent that both clinoptilolite and mesolite have smaller regions of stability at 100 °C than at 25 °C, and that Ca end-member phillipsite replaces heulandite at low activities of silica.

The effects of variable Al activity at 25 °C can be observed in Figure 8. Clinoptilolite is not stable at high Al activities corresponding to gibbsite saturation (Fig. 8d) but appears with decreasing Al activities (Figs. 8a–8c). Its stability field maximizes at an intermediate Al activity constrained by the coexistence of amorphous silica and pyrophyllite (cf. smectite) (Fig. 8b) and then becomes smaller with further decrease in Al activity (Fig. 8a). Similar less conspicuous trends exist for heulandite. The stability field of mesolite, on the other hand, increases with rising Al activity and maximizes at gibbsite saturation, where the clinoptilolite, heulandite, mordenite, and phillipsite fields disappear (Fig. 8d). Note that circles representing Ca and Na concentrations of J-13 well water plot close to the join of mordenite, clinoptilolite, and amorphous silica (Fig. 8a), and with heulandite, mordenite, and clinoptilolite (Fig. 8b), which are consistent with mineral assemblages observed at Yucca Mountain. Ef-

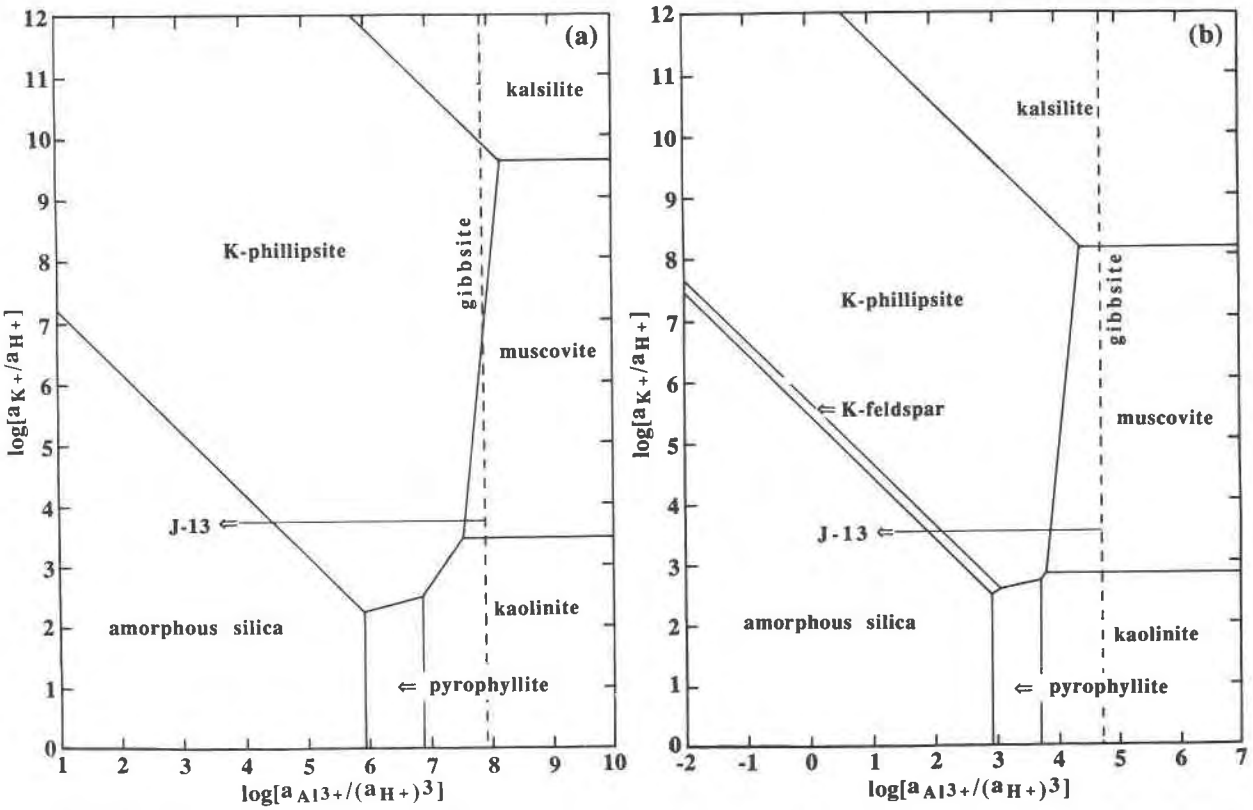

Fig. 5. Activity diagrams for the system K-Al-Si plus H_2O balanced with respect to Si (**a**) at 25 °C; and (**b**) at 100 °C.

fects of temperature may be seen in Figures 9a–9c, which show that the clinoptilolite and heulandite stability fields decrease with increasing temperature and appear only at low Al activities. At 150 °C with Al activity corresponding to coexisting pyrophyllite and amorphous silica, clinoptilolite, but not heulandite, still has a small stability field (Fig. 9d). Thus, alkali-rich clinoptilolites are expected to persist to at least 150 °C, as indicated by their occurrence in drill holes at Yellowstone (Keith et al., 1978; Sturchio et al., 1989), but under a significantly reduced range of Al activities.

In Figures 10a and 10b, the system Ca-Na-K-Al-Si is represented at 25 °C with $\log(a_{K^+})/(a_{H^+})$ replacing $\log(a_{Na^+})/(a_{H^+})$ on the x-axis and albite replacing potassium feldspar as the saturation phase. Figure 10a is balanced on Al, and amorphous silica is the saturation phase, whereas Figure 10b is balanced on Si with Al^{3+} activity controlled by coexisting amorphous silica plus pyrophyllite. These two representative activity diagrams based on K^+ activities are very similar to their Na-counterparts, except that K–end-member–silicate phases replace Na–end-member–silicate minerals. The stability field of clinoptilolite is again largest at high silica activities, intermediate Al^{3+} activities, and low temperatures.

Activity diagrams for clinoptilolites of variable compositions

As noted earlier, clinoptilolite compositions vary considerably at Yucca Mountain (Fig. 1). Therefore, activity diagrams were calculated for clinoptilolites of variable Na-Ca, K-Ca, and Ca-Mg contents (Fig. 1), and the results are shown in Figure 11. The stability fields are identified in Figure 11a, which is related to the activity diagram in Figure 8b, where Si is balanced and Al activities are constrained by the assemblage pyrophyllite + amorphous silica + potassium feldspar, which corresponds to conditions of maximum clinoptilolite stability at 25 °C.

Figure 11b shows that with increasing atomic substitution of Na in clinoptilolite, the clinoptilolite stability field narrows. Conversely, the clinoptilolite stability field widens for clinoptilolites with higher Ca contents and merges into the heulandite field. Clinoptilolites more sodic than $Na_{0.56}Ca_{1.5}$ are no longer in equilibrium with J-13 well water, suggesting that ground water with higher Na and lower Ca concentrations, perhaps derived from altered vitric tuffs (White et al., 1980), is necessary to stabilize sodic clinoptilolites.

K has the opposite effect on the clinoptilolite stability

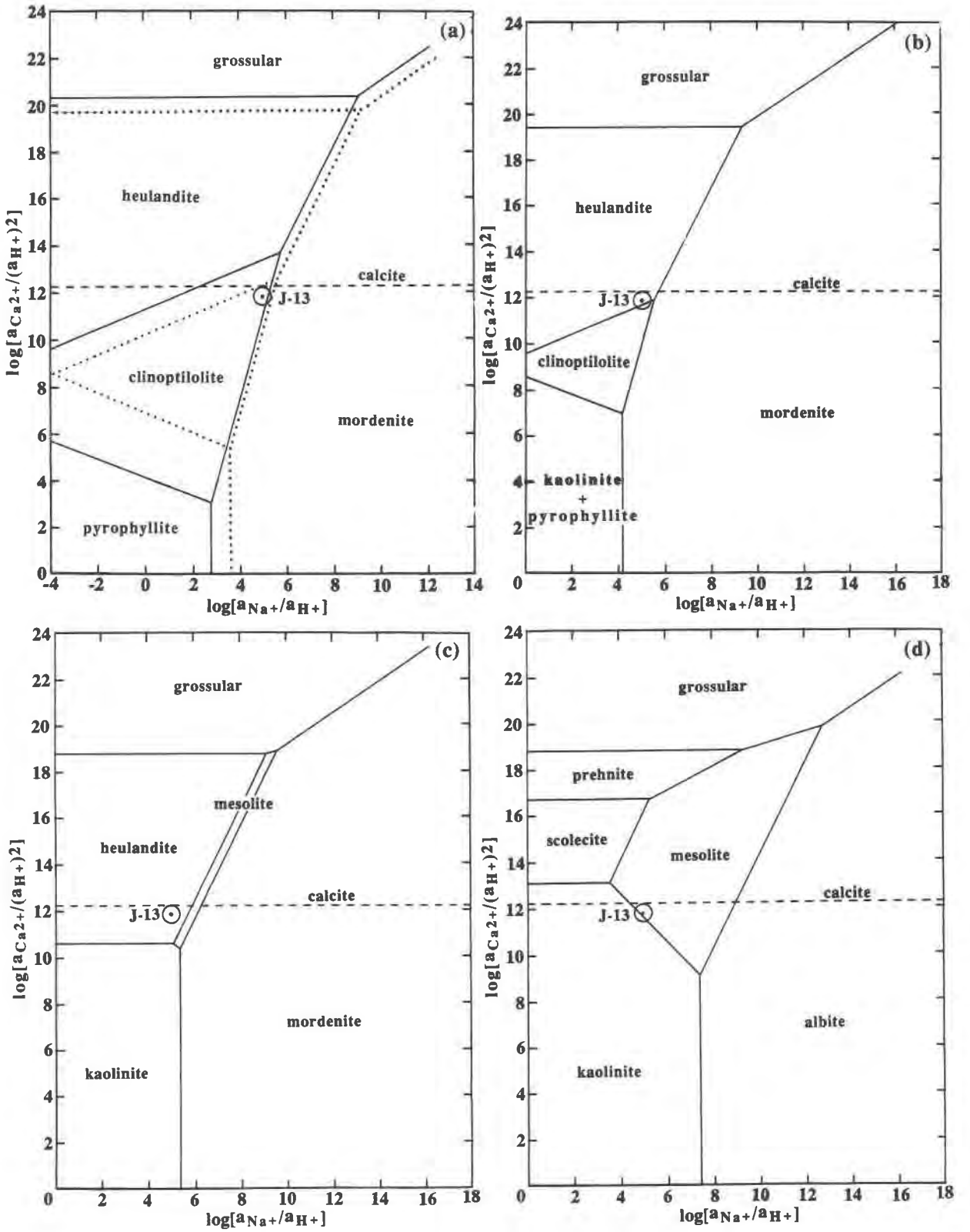

Fig. 6. Activity diagrams for the system Ca-Na-K-Al-Si plus H_2O balanced with respect to Al at 25 °C for different silica activities: (**a**) amorphous silica and J-13 well water (dotted lines), (**b**) pyrophyllite-kaolinite, (**c**) cristobalite, and (**d**) quartz. Saturation phases also include potassium feldspar, hematite, and Ca end-member saponite.

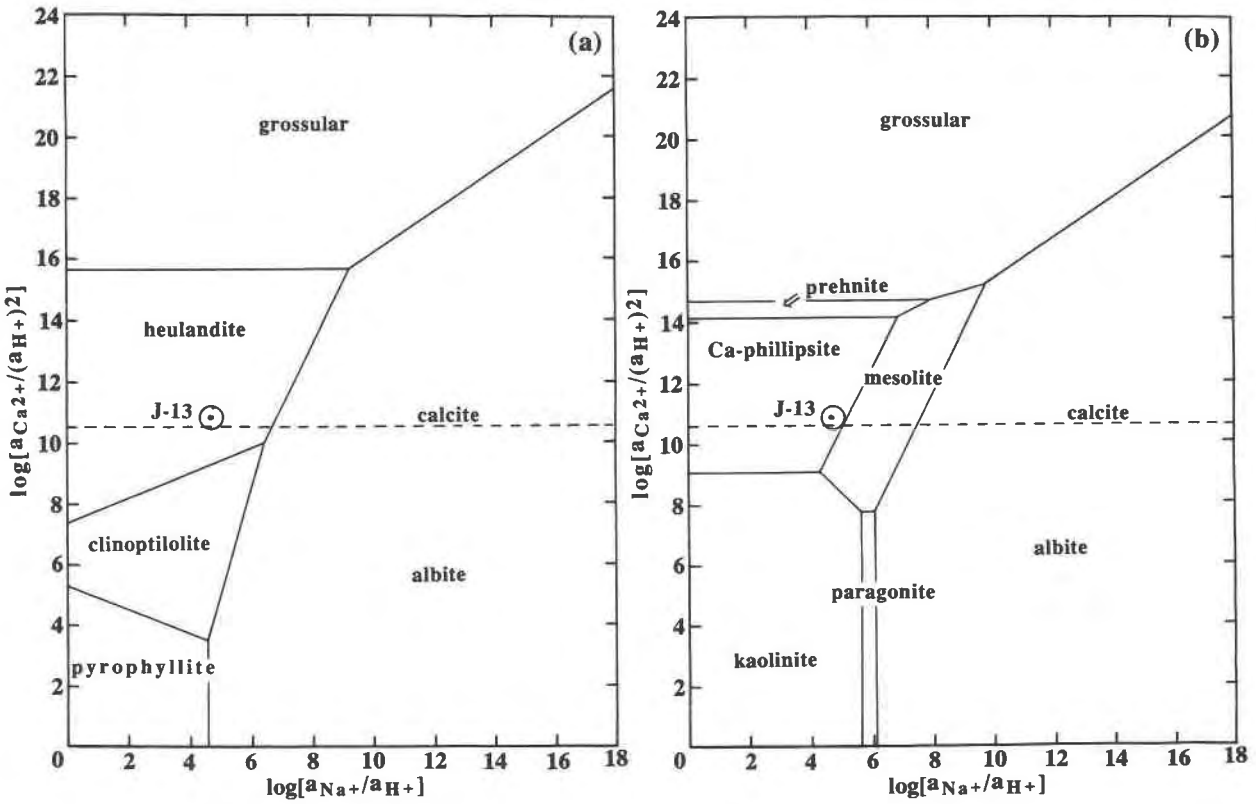

Fig. 7. Activity diagrams for the system Ca-Na-K-Al-Si plus H_2O balanced with respect to Al at 100 °C for different silica activities: (a) amorphous silica, and (b) quartz.

field (Fig. 11c), which widens considerably with increasing atomic substitution of K for Ca. Clinoptilolites less potassic than $K_{0.98}Ca_{1.5}$ would no longer be in equilibrium with J-13 well water. In contrast, replacement of Ca by Mg in clinoptilolite displaces its stability field to lower Ca activities (Fig. 11d). Clinoptilolites more magnesian than $Ca_{1.7}Mg_{1.03}$ would not be in equilibrium with J-13 well water.

Discussion

The activity diagrams demonstrate that the formation of clinoptilolite is favored by SiO_2 activities higher than allowed for by the presence of quartz. This is demonstrated by Figure 6 and is achieved, for example, when clinoptilolite coexists with opal in diagenetically altered volcanic glasses. Heulandite, however, can exist in the presence of opal and cristobalite but not quartz. Such assemblages are commonly observed in vitric tuff samples from drill cores at Rainier Mesa and Yucca Mountain (Benson, 1976; White et al., 1980; Broxton et al., 1987) and from surface desert pavement and outcrop locations (Burns et al., 1990).

Clinoptilolite has a maximum stability field at an intermediate Al activity value but shrinks with either increasing or decreasing activities of Al. This is indicated by Figure 8, in which the clinoptilolite stability field is largest when Al activities are controlled by the assemblage amorphous silica + pyrophyllite (cf. smectite) (Fig. 8b). Furthermore, since the composition of J-13 well water appears to be approximately in equilibrium with respect to calcite, the J-13 Ca^{2+}/Na^+ points plotted in Figures 8b and 8c suggest that if J-13 well water is in equilibrium with clinoptilolite, then the Al activities should lie between the values for kaolinite-pyrophyllite and pyrophyllite–amorphous silica. Such Al activities also indicate that J-13 well water could be in equilibrium with other zeolites represented on the activity diagrams, including heulandite and mordenite (Fig. 6b) and possibly mesolite (Figs. 8c and 10b), particularly when the stability field of Na-rich clinoptilolites is diminished (Fig. 11b). These observations for calcic clinoptilolite, heulandite, and mordenite correlate with the occurrence of these zeolites as fracture linings in welded and devitrified tuffs and in basal vitrophyres in the vadose zone throughout Yucca Mountain (Broxton et al., 1987; Levy, 1984). Chabazite occurring with coatings of fine-grained heulandite in fractured vitrophyre below the water table in the J-13 well (Carlos, 1989) does not appear to have a stability field

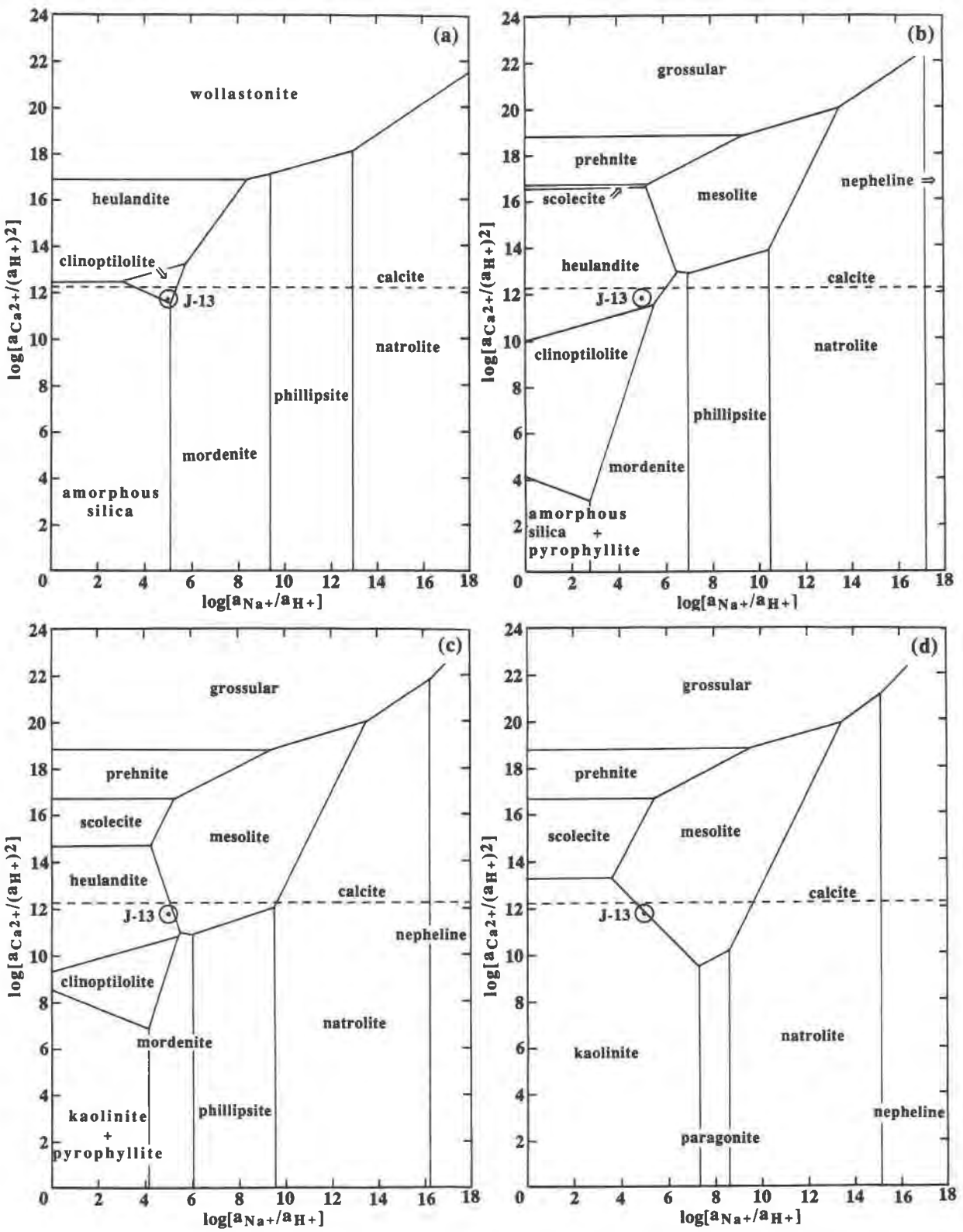

Fig. 8. Activity diagrams for the system Ca-Na-K-Al-Si plus H_2O balanced with respect to Si at 25 °C for different Al activities: (a) low Al activity corresponding to line I in Fig. 2, (b) pyrophyllite-amorphous silica, (c) kaolinite-pyrophyllite, and (d) gibbsite. Saturation phases again include potassium feldspar, hematite, and Ca end-member saponite.

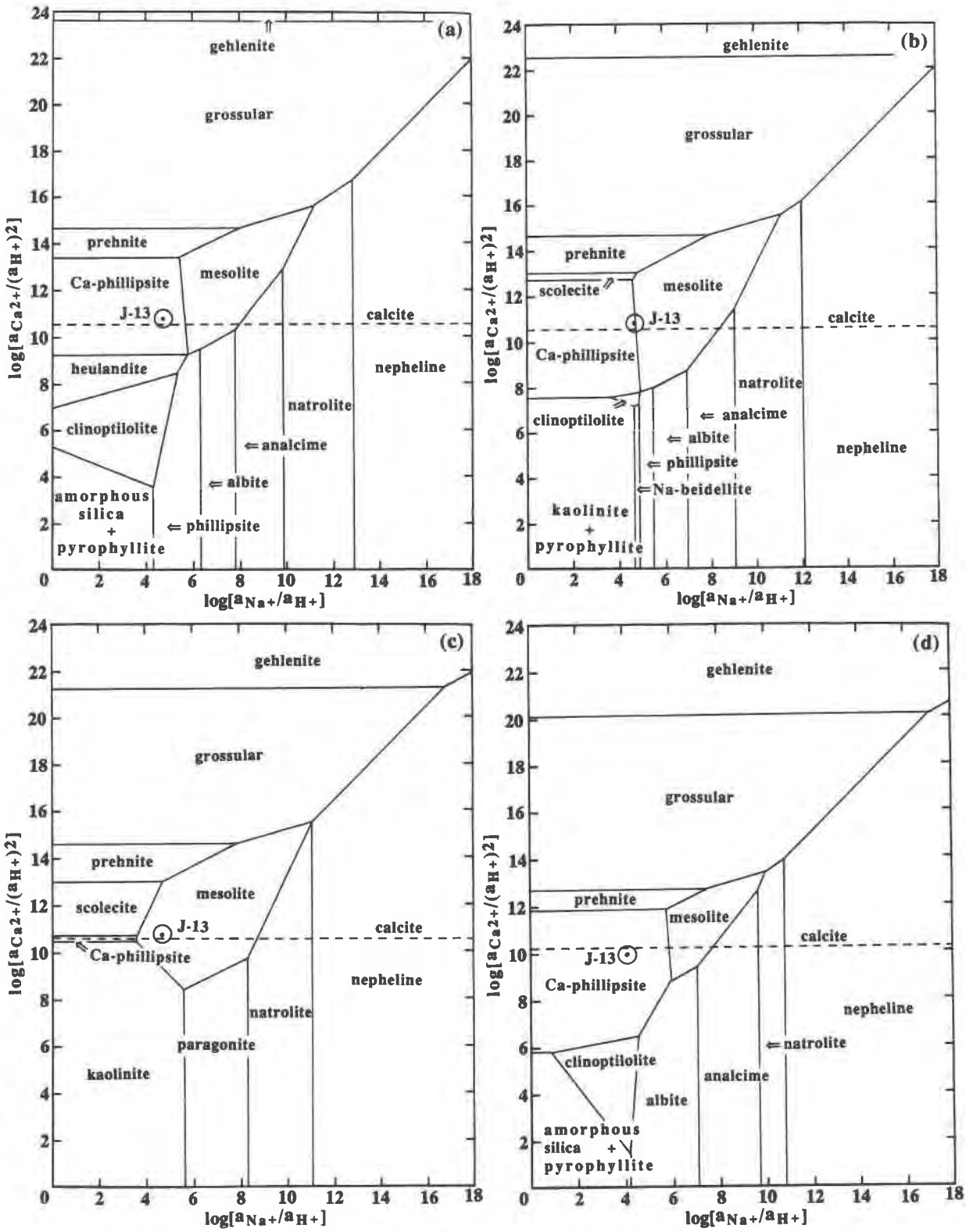

Fig. 9. Activity diagrams for the system Ca-Na-K-Al-Si plus H_2O at elevated temperatures balanced with respect to Si for different Al activities: (**a**) pyrophyllite-amorphous silica at 100 °C, (**b**) kaolinite-pyrophyllite at 100°C; (**c**) gibbsite at 100 °C, and (**d**) pyrophyllite-amorphous silica at 150 °C.

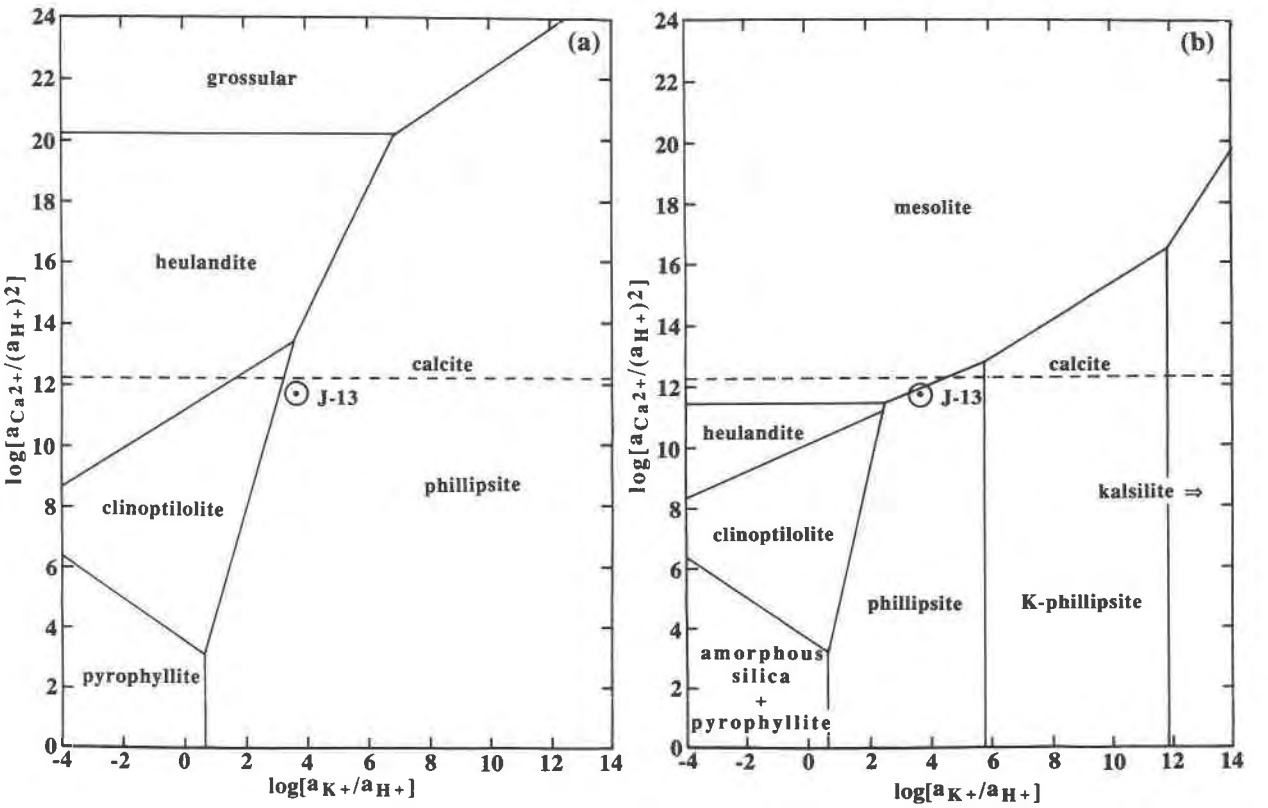

Fig. 10. Activity diagrams based on K and Ca activities in the system Ca-Na-K-Al-Si plus H_2O at 25 °C (**a**) balanced with respect to Al with silica saturation by amorphous silica, and (**b**) balanced with respect to Si with Al saturation by pyrophyllite + amorphous silica. Saturation phases include albite, hematite, and Ca end-member saponite.

and may be metastable with respect to mesolite or scolecite.

The clinoptilolite stability field decreases with increasing temperature between 25 and 150 °C (Figs. 7a, 9a, 9b, and 9d) and likely disappears by 200 °C. This correlates with hydrothermal experiments (Boles, 1971; Knauss et al., 1985a, 1985b; Hawkins et al., 1978) and observed geological occurrences of clinoptilolite (Hay, 1966; Hay and Sheppard, 1977). Potassic clinoptilolites have been identified at 120–140 °C in drill cores from the Yellowstone hydrothermal environment (Keith et al., 1978; Sturchio et al., 1989), however, correlating with the increased stability field of K-rich clinoptilolites (see Fig. 11c).

Zeolite diagenetic zones have been suggested for alteration of vitric tuffs based on the appearance and disappearance of clinoptilolite in buried pyroclastic deposits (Iijima, 1975, 1980; Smyth, 1982). Zone I, for example, is characterized by large-scale preservation of glass in vitric tuffs above the water table and incipient alteration of glass shards, particularly in groundmass, to smectite and opal. The Topopah Spring Member at Yucca Mountain, lying well above the water table, falls into Zone I. However, Ca-rich clinoptilolites occur in fractures through lower welded tuff and vitrophyre horizons of the Topopah Spring Member and may be indicative of groundwater interactions, perhaps with microcrystalline devitrified tuffs, which produce relatively high concentrations of dissolved Ca^{2+}, Na^+, and HCO_3 in fracture-flow water (White et al., 1980). The activity diagrams calculated for 25 °C consistently show that calcic clinoptilolites are stable in the presence of fracture-flow J-13 well water originating from microcrystalline devitrified Topopah Spring Member tuffs, even though such zeolites have not been observed as fracture-lining minerals at this level in J-13 drill cores (Carlos, 1989). The abundance of drusy quartz coating fractures at that level (Carlos, 1989) may depress the silica activity below that necessary to crystallize clinoptilolite (and heulandite).

Diagenetic Zone II, which characterizes the bedded tuffs below the Topopah Spring Member, represents extensive zeolitization of vitric tuffs to clinoptilolite-bearing assemblages and is promoted by water enriched in alkali cations and by slightly elevated temperatures (Smyth, 1982). Progressive hydration and dissolution reactions of the rhyolitic vitric tuffs increase the concentrations of SiO_2, Na^+,

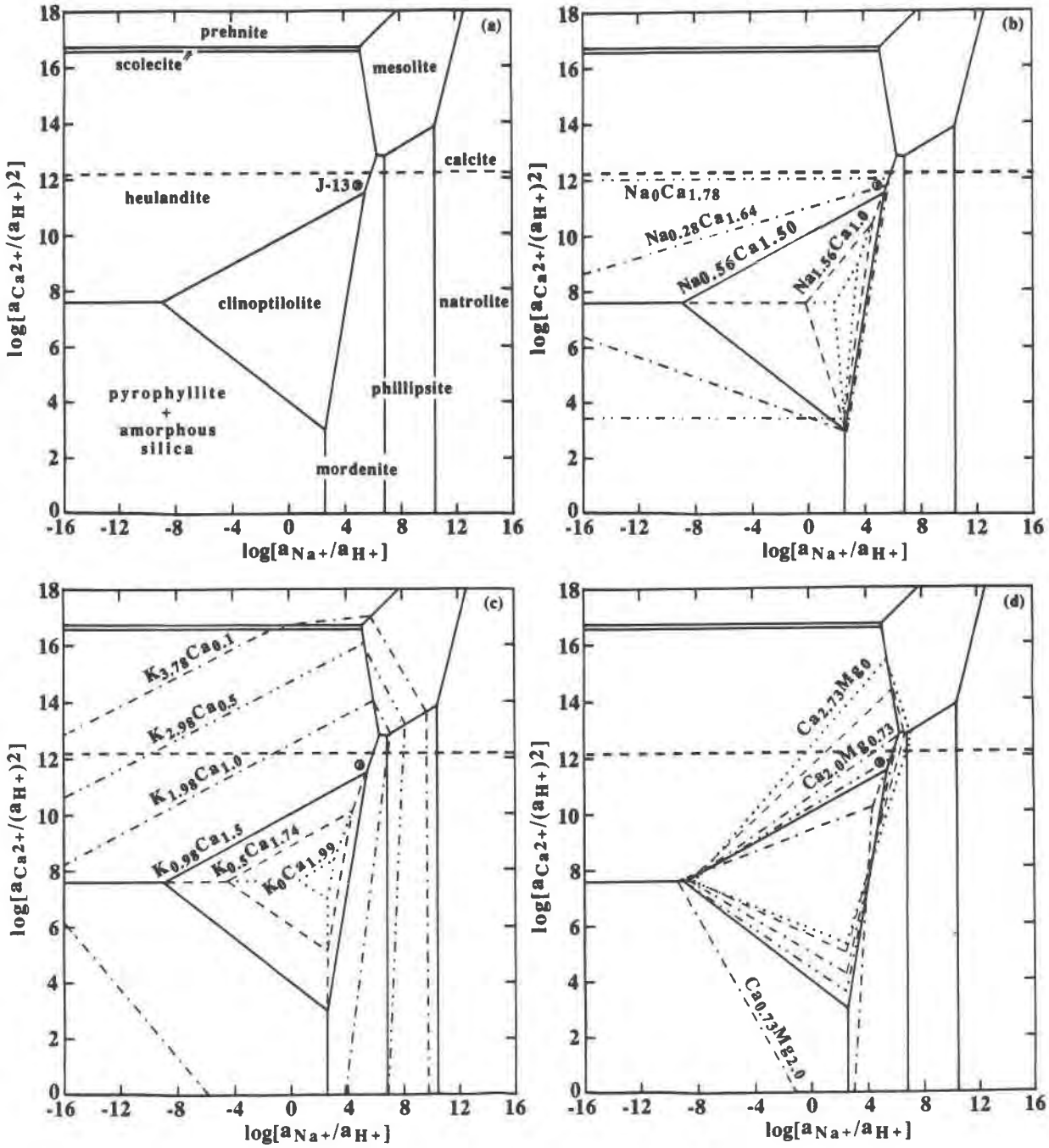

Fig. 11. Activity diagrams for clinoptilolites having variable cation compositions. The calculated stability fields at 25 °C correspond to aluminum saturation by pyrophyllite plus amorphous silica and are balanced with respect to Si (compare Fig. 7b). (**a**) reference diagram for the clinoptilolite composition $Na_{0.56}K_{0.98}Ca_{1.50}Mg_{1.23}$; (**b**) Ca-Na variations: -·-·-·- = $Na_0Ca_{1.78}$, -·-·- = $Na_{0.28}Ca_{1.64}$, —— = $Na_{0.56}Ca_{1.5}$, ----- = $Na_{1.56}Ca_{1.0}$, ····· = $Na_{2.56}Ca_{0.5}$. (**c**) K-Ca variations: -·-·-·- = $K_{3.98}Ca_{0.1}$, -·-·-·- = $K_{2.98}Ca_{0.5}$, -·-·- = $K_{1.98}Ca_{1.0}$, —— = $K_{0.98}Ca_{1.5}$, ----- = $K_{0.5}Ca_{1.74}$, ····· = $K_0Ca_{1.99}$. (**d**) Ca-Mg variations: ····· = $Ca_{2.73}Mg_0$, ----- = $Ca_{2.5}Mg_{0.23}$, -·-·- = $Ca_{2.0}Mg_{0.73}$, -·-·-·- = $Ca_{1.7}Mg_{1.03}$, —— = $Ca_{1.5}Mg_{1.23}$, -·-·-·-·- = $Ca_{0.73}Mg_{2.0}$.

and ultimately K^+ in ground water (White et al., 1980) from which clinoptilolite-clay silicate-opal assemblages are derived. The presence of Ca-poor, K-Na-rich clinoptilolites in diagenetic Zone II conforms with the activity diagrams, which consistently show the clinoptilolite stability field moving away from J-13 well-water compositions at elevated temperatures, as well as by increased Na, but depleted Ca, concentrations in ground water.

Deeper drill cores through Yucca Mountain have yielded analcime instead of clinoptilolite, which is indicative of diagenetic Zone III, whereas Zone IV is represented by the breakdown of analcime to albite. It has been suggested that the clinoptilolite-analcime transition depends on the concentration of dissolved Na, and the Zone II–Zone III boundary was estimated to lie between 100 and 150 °C for present-day ground-water compositions at Yucca Mountain (Smyth, 1982). However, Kerrisk (1983) concluded from reaction-path calculations that the clinoptilolite-analcime transition is controlled by the activity of dissolved silica. Mordenite coexists with clinoptilolite in zeolitized tuffs at Yucca Mountain. Textural evidence (Sheppard et al., 1988) suggests that some mordenites have formed at the expense of clinoptilolite during late-stage dissolution, and this observation is consistent with our activity diagrams. However, mordenite also persists at higher temperatures (~170 °C) than clinoptilolite (~140 °C) in drill holes through the Yellowstone hydrothermal environment (Keith et al., 1978; Sturchio et al., 1989), but this observation cannot be correlated with activity diagrams calculated at elevated temperatures because of lack of thermodynamic data for mordenite. The inability to include mordenite in such activity diagrams may be responsible for the apparent stability fields of albite or phillipsite abutting the clinoptilolite field instead of analcime in the diagrams calculated at 100 °C (Figs. 7a and 9a) and 150 °C (Fig. 9d).

Effects of temperature on the calcic clinoptilolite and heulandite stability fields, together with occurrences of K-Na-rich clinoptilolites at elevated temperatures (Sturchio et al., 1989), suggest that calcic zeolites are most vulnerable to thermal decomposition (cf. Figs. 8a and 8d). Such Ca-rich zeolites occur in fractures (Carlos, 1985) and in the vitrophyre at the base of the Topopah Spring Member tuff at Yucca Mountain (Levy, 1984). The density of fractures is highest in the densely welded tuff horizon in the Topopah Spring Member (Scott et al., 1983) where siting of the proposed nuclear waste repository is planned. In the vicinity of the heat envelope that would surround radioactive waste buried there, fluid temperatures could exceed 150 °C within a radius of 10 m from the proposed repository horizon (Travis et al., 1984; U.S. DOE, 1988, p. 4–118), and thereby affect the thermal stability of calcic zeolites in the fractures and underlying basal vitrophyre.

Several observed reactions suggested by phase assemblages in weathered vitric tuffs (Benson, 1976; White et al., 1980; Burns et al., 1990) can be demonstrated on the activity diagrams. For example, the reaction of glass + clay silicates to clinoptilolite + opal plots at the intersection of amorphous silica + pyrophyllite + mordenite + clinoptilolite in Figures 6a and 8b, but requires lower calcium activities in the coexisting fluid than that of J-13 well water. Low Ca and slightly reduced K activities of rainwater would account for the assemblage glass + clay silicates + opal + clinoptilolite + authigenic potassium feldspar forming on weathered vitric tuffs at outcrops and in detritus forming desert pavement (Burns et al., 1990). The assemblage of clinoptilolite + calcite + opal also found in weathered vitric tuffs is represented on Figure 8a, requiring, however, very low activities of Al.

Conclusions

The calculated activity diagrams presented here quantify observed field occurrences and verify deductions made about the stability of clinoptilolite during burial diagenesis of vitric tuffs. The coexistence of clinoptilolite with opal correlates with its calculated wide stability field in aqueous solutions saturated with amorphous silica. Clinoptilolite-smectite assemblages indicate that the zeolite crystallized from ground water with dissolved Al concentrations lower than saturation values with respect to gibbsite and lower than the reported measurements of J-13 well water. Calcic clinoptilolites associated with calcite are consistent with crystallization from fracture-flow ground water containing Ca^{2+} and HCO_3^- derived from incipient dissolution of microcrystalline devitrified tuffs. Alkali-rich clinoptilolites, on the other hand, correlate with ground water having elevated Na^+ and K^+ but depleted Ca^{2+} concentrations, which are associated with altered vitric tuffs. Although the crystallization of clinoptilolite may be promoted by ground water enriched in silica and alklai metals, the clinoptilolite stability field diminishes appreciably between 25 and 150 °C, correlating with burial diagenetic reactions, and confirming doubts (Smyth, 1982) about the thermal stability of calcic clinoptilolites close to buried radioactive waste. Questions remain, however, concerning the stability of calcic versus K-Na-rich clinoptilolites at elevated temperatures and the effects of compositional variations in heulandite and mordenite. Recently revised thermodynamic properties of heulandite (Johnson et al., 1989) and limited information on thermal stability limits of mordenite (Kusakabe et al., 1981) may constrain our ongoing calculations of zeolite activity diagrams.

Acknowledgments

We gratefully acknowledge the assistance of Drs. M. E. Morgenstein, C. L. Johnson, and D. L. Shettel, who reviewed early drafts of the manuscript and provided information about ground-water chemistry at Yucca Mountain. Helpful comments on the original manuscript were received from Drs. J. A. Apps, D. L. Bish, J. G. Liou, W. M. Murphy, J. K. Bohlke, and an anonymous reviewer. Dr. J. F. Kerrisk kindly provided his report on clinoptilolite stability field calculations. The study was funded by the State of Nevada, Nuclear Waste Project Office, under a Department of Energy grant from the Nuclear Waste Fund.

References cited

Benson, L.V. (1976) Mass transport in vitric tuffs of Rainier Mesa, Nye County, Nevada. U.S. Energy Research and Development Administration, Nevada, Report NVO-1253-10.

Bish, D.L. (1989) Evaluation of past and future alterations in tuff at Yucca Mountain, Nevada, based on the clay mineralogy of drill cores USW G-1, G-2, and G-3. U.S. National Technical Information Service, Report LA-10667, 40 p.

Bish, D.L., Ogard, A.L., Vaniman, D.T., and Benson, L. (1984) Miner-

alogy-petrology and groundwater chemistry of Yucca Mountain Tuffs. Materials Research Society Symposium Research Proceedings, 26, 283–291.

Boles, J.R. (1971) Synthesis of analcime from natural heulandite and clinoptilolite. American Mineralogist, 56, 1724–1734.

Bowers, T.S., Jackson, K.J., and Helgeson, H.C. (1984) Equilibrium activity diagrams for coexisting minerals and aqueous solutions at pressures and temperatures to 5 kb and 600 °C. Springer-Verlag, New York.

Broxton, D.E., Bish, D.L., and Warren, R.G. (1987) Distribution and chemistry of diagenetic minerals at Yucca Mountain, Nye County, Nevada. Clays and Clay Minerals, 35, 89–110.

Broxton, D.E., Warren, R.G., Hagan, R.C., and Luedemann, G. (1986) Chemistry of diagenetically altered tuffs at a potential nuclear waste repository, Yucca Mountain, Nye County, Nevada. U.S. National Technical Information Service, Report LA-10802, 160 p.

Broxton, D.E., Byers, F.M., Jr., and Warren, R.G. (1989) Petrography and phenocryst chemistry of volcanic units at Yucca Mountain, Nevada: A comparison of outcrop and drill hole samples. U.S. National Technical Information Service, Report LA-11503, 65 p.

Burns, R.G., Bowers, T.S., Wood, V.J., Blundy, J.D., and Morgenstein, M.E. (1990) Reactivity of zeolites forming in vitric tuffs in the unsaturated zone at Yucca Mountain, Nevada. In Proceedings of nuclear waste isolation in the undersaturated zone, Focus '89, p. 101–112. American Nuclear Society, La Grange Park, IL.

Carlos, B.A. (1985) Minerals in fractures of the unsaturated zone from drill core USW G-4, Yucca Mountain, Nye County, Nevada. U.S. National Technical Information Service, Report LA-10415, 55 p.

——— (1989) Fracture-coating minerals in the Topopah Spring Member and Upper Tuff of Calico Hills from drill hole J-13. U.S. National Technical Information Service, Report LA-11504, 20 p.

Chen, C.-H. (1975) A method of estimation of standard free energies of formation of silicate minerals at 298.15 °K. American Journal of Science, 275, 801–817.

Daniels, W.R., et al. (29 coauthors) (1982) Summary report on the geochemistry of Yucca Mountain and environs. U.S. National Technical Information Service, Report LA-9328.

Delany, J.M. (1985) Reaction of Topopah Spring tuff with J-13 water: A geochemical modeling approach using the EQ3/6 reaction path code. U.S. National Technical Information Service, Report UCRL-53631.

Hawkins, D.B., Sheppard, R.A., and Gude, A.J., III (1978) Hydrothermal synthesis of clinoptilolite and comments on the assemblage phillipsite-clinoptilolite-mordenite. In L.B. Sands and F.A. Mumpton, Eds., Natural zeolites, p. 337–349. Pergamon Press, New York.

Hay, R.L. (1966) Zeolites and zeolite reactions in sedimentary rocks. Geological Society of America Special Paper 85, p. 130–146.

Hay, R.L., and Sheppard, R.A. (1977) Zeolites in open hydrologic systems. In F.A. Mumpton, Ed., Mineralogy and geology of natural zeolites. Mineralogical Society of America Reviews in Mineralogy, 4, 92–102.

Hemingway, B.S., and Robie, R.A. (1984) Thermodynamic properties of zeolites: Low temperature heat capacities and thermodynamic functions of phillipsite and clinoptilolite. Estimates of the thermochemical properties of zeolitic water at low temperatures. American Mineralogist, 69, 692–700.

Hoover, D.L. (1968) Genesis of zeolites, Nevada Test Site. Geological Society of America Memoir 110, 275–284.

Iijima, A. (1975) Effect of pore water to clinoptilolite-analcime-albite reaction series. Journal of the Faculty of Science, University of Tokyo, Series II, 19, 133–147.

——— (1980) Geology of natural zeolites and zeolitic rocks. In L.V.C. Rees, Ed., Proceedings of the Fifth International Conference on Zeolites, p. 103–118. Heyden & Co., London.

Johnson, G.K., Flotow, H.E., O'Hare, P.A.G., and Wise, W.S. (1982) Thermodynamic studies of zeolites: Analcime and dehydrated analcime. American Mineralogist, 67, 736–748.

——— (1983) Thermodynamic studies of zeolites: Natrolite, mesolite, and scolecite. American Mineralogist, 68, 1134–1145.

——— (1985) Thermodynamic studies of zeolites: Heulandite. American Mineralogist, 70, 1065–1071.

——— (1989) Thermodynamic studies of zeolites: Heulandite: Erratum. American Mineralogist, 74, 697.

Keith, T.E.C., White, D.E., and Beeson, M.H. (1978) Hydrothermal alteration and self-sealing in Y-7 and Y-8 drill holes in northern part of Upper Geyser Basin, Yellowstone National Park, Wyoming. U.S. Geological Survey Professional Paper 1054-A, A1–A26.

Kerrisk, J.F. (1983) Reaction-path calculations of groundwater chemistry and mineral formation at Rainier Mesa, Nevada. U.S. National Technical Information Service, Report LA-9912-MS, 41 p.

Kerrisk, J.F. (1987) Groundwater chemistry at Yucca Mountain, Nevada, and vicinity. U.S. National Technical Information Service, Report LA-10929, 113 p.

Knauss, K.G., Beiringer, W.J., and Peifer, D.W. (1985a) Hydrothermal interaction of crushed Topopah Spring tuff and J-13 water at 90, 150, and 250 °C using Dickson-type, gold-bag rocking autoclaves. U.S. National Technical Information Service, UCRL-53630, 27 p.

Knauss, K.G., Delany, J.M., Beiringer, W.J., and Peifer, D.W. (1985b) Hydrothermal interaction of Topopah Spring Tuff with J-13 water as a function of temperature. Materials Research Society Symposium Proceedings, 27, 539–546.

Kusakabe, H., Minato, H., Utada, M., and Yamanaka, T. (1981) Phase relations of clinoptilolite, mordenite, analcime and albite with increasing pH, sodium ion concentration and temperature. Scientific Papers of the College of General Education, University of Tokyo, 31, 39–59.

Levy, S.S. (1984) Studies of altered vitrophyre for the prediction of nuclear waste repository-induced thermal alteration at Yucca Mountain, Nevada. Materials Research Society Symposium Proceedings, 26, 959–966.

Moncure, G.K., Surdam, R.C., and McKague, H.L. (1981) Zeolite diagenesis below Pahute Mesa, Nevada Test Site. Clays and Clay Minerals, 29, 385–396.

Moore, D.E., Morrow, C.A., and Byerlee, J.D. (1986) High-temperature permeability and groundwater chemistry of some Nevada Test Site tuffs. Journal of Geophysical Research, 82, 2163–2171.

Ogard, A.E., and Kerrisk, J.F. (1984) Groundwater chemistry along flow paths between a proposed repository site and the accessible environment. U.S. National Technical Information Service, Report LA-10188.

Ogard, A.E., Wolfsberg, K., Daniels, W.R., Kerrisk, J., Rundberg, R.S., and Thomas, K.W. (1984) Retardation of radionuclides by rock units along the flow path to the accessible environment. Materials Research Society Symposium Proceedings, 26, 329–336.

Oversby, V.M. (1985) The reaction of Topopah Spring tuff with J-13 water at 90 °C and 150 °C—Samples from drill cores USW G-1, USW GU-3, USW G-4, and UE-25h#1. U.S. National Technical Information Service, Report UCRL-53629, 26 p.

Scott, R.B., Spengler, R.W., Diehl, S., Lappin, A.R., and Chornack, M.P. (1983) Geologic character of tuffs in the unsaturated zone at Yucca Mountain, southern Nevada. In J.W. Mercer, P.S.C. Rao, and I.W. Wendell, Eds., Role of the unsaturated zone in radioactive and hazardous waste disposal, p. 289–335. Ann Arbor Science, Ann Arbor, Michigan.

Sheppard, R.A., and Gude, A.J., III (1973) Zeolites and associated authigenic silicate minerals in tuffaceous rocks of the Big Sandy formation, Mohave County, Arizona. U.S. Geological Survey Professional Paper 830.

Sheppard, R.A., Gude, A.J.,III and Fitzpatrick, J.J. (1988) Distribution, characterization, and genesis of mordenite in Miocene silicic tuffs at Yucca Mountain, Nye County, Nevada. U.S. Geological Survey Bulletin 1777, 22 p.

Smyth, J.R. (1982) Zeolite stability constraints on radioactive waste isolation in zeolite-bearing volcanic rocks. Journal of Geology, 90, 195–201.

Sturchio, N.C., Bohlke, J.K., and Binz, C.M. (1989) Radium-thorium disequilibrium and zeolite-water ion exchange in a Yellowstone hydrothermal environment. Geochimica et Cosmochimica Acta, 53, 1025–1034.

Thomas, K.W. (1987) Summary of sorption measurements performed with Yucca Mountain, Nevada, tuff samples and water from well J-13. U.S. National Technical Information Service, Report LA-10960, 99 p.

Travis, B.J., Hodson, S.W., Nuttall, H.E., Cook, T.L., and Rundberg, R.S. (1984) Numerical simulation of flow and transport in fractured tuff. Materials Research Society Symposium Proceedings, 26, 1039–1046.

U.S. Department of Energy (1988) Site characterization plan, Yucca Mountain Site, Nevada, research and development area, Nevada, Report DOE/RW-0160, 8 vols.

White, A.F., Claassen, H.C., and Benson, L.V. (1980) The effect of dissolution of volcanic glass on the water chemistry in a tuffaceous aquifer, Rainier Mesa, Nevada. U.S. Geological Survey Water-Supply Paper 1535-Q, 33 p.

Wolery, T.J. (1983) EQ3NR, a geochemical program for geochemical aqueous speciation-solubility calculations. U.S. National Technical Information Service, UCRL-5, Distribution Category UC-70.

Yang, I.C., Turner, A.K., Sayre, T.M., and Montazer, P. (1988) Triaxial-compression extraction of pore water from unsaturated tuff, Yucca Mountain, Nevada. U.S. Geological Survey Water-Resources Investigations Report 88-4189, 68 p.

Manuscript received November 28, 1988
Manuscript accepted February 2, 1990